applied sciences

MDPI

Article

Conversion of NO_x over Aluminosilicate Cu-CHA Zeolite Catalysts Synthesized Free of Organic Structure-Directing Agents

Galal A. Nasser [1,*], Haruna Adamu [2,3], Akolade I. Bakare [1], Mohammad A. Sanhoob [1], Huawang Zhao [4], Zain H. Yamani [1], Oki Muraza [1], Emad Shafeai [5] and Johannes W. Schwank [4,*]

1 Center of Excellence in Nanotechnology and Chemical Engineering Department, King Fahd University of Petroleum and Minerals, Dhahran 31261, Saudi Arabia; aibakare@kfupm.edu.sa (A.I.B.); sanhoob@kfupm.edu.sa (M.A.S.); zhyamani@kfupm.edu.sa (Z.H.Y.); oki.muraza@pertamina.com (O.M.)
2 Department of Environmental Management Technology, Abubakar Tafawa Balewa University, Yalwa Campus, Bauchi 740272, Nigeria; hadamu2@atbu.edu.ng
3 Department of Chemistry, Abubakar Tafawa Balewa University, Yalwa Campus, Bauchi 740272, Nigeria
4 Department of Chemical Engineering, University of Michigan, Ann Arbor, MI 48109, USA; hwzhao@hqu.edu.cn
5 Research and Development Center, Saudi Aramco, Dhahran 31311, Saudi Arabia; emad.shafei@aramco.com
* Correspondence: galal.nasser@kfupm.edu.sa (G.A.N.); schwank@umich.edu (J.W.S.)

Featured Application: Catalytic NOx emission control.

Abstract: Cu-CHA zeolites have proven to be effective for NO_x reduction, but a drawback in using CHA zeolites is the cost associated with using expensive organic structure-directing agents. To overcome this drawback, we are reporting here the synthesis of Cu-CHA zeolite catalysts in both their NH_4-form as well as K-form that do not require the use of organic structure-directing agents. After comprehensive characterization by XRF, XRD, ^{27}Al NMR spectroscopy, FE-SEM, SEM/EDS, N_2-adsorption/desorption, NH_3-TPD, H_2-TPR, and XPS, the zeolite catalysts were tested for NO_x conversion by NH_3-selective catalytic reduction (NH_3-SCR). Cu-NH_4-CHA zeolite catalysts exhibited remarkable activity and thermal stability over a wide temperature window, outperforming their counterpart K-forms. Among the NH_4-forms of CHA zeolite catalysts, the 0.1 M Cu-NH_4-CHA showed the best catalytic performance, achieving 50% NO_x conversion at a temperature as low as 192 °C, and reaching full conversion of NO_x at 261 °C. These Cu-based CHA zeolite catalysts are promising thanks to their environmentally friendly synthesis and offer the opportunity of maximizing $DeNO_x$ strategies in applications for NO_x pollution abatement.

Keywords: organic structure-directing agent; selective catalytic reduction; Chabazite; zeolite

Citation: Nasser, G.A.; Adamu, H.; Bakare, A.I.; Sanhoob, M.A.; Zhao, H.; Yamani, Z.H.; Muraza, O.; Shafeai, E.; Schwank, J.W. Conversion of NO_x over Aluminosilicate Cu-CHA Zeolite Catalysts Synthesized Free of Organic Structure-Directing Agents. *Appl. Sci.* **2023**, *13*, 13001. https://doi.org/10.3390/app132413001

Academic Editors: Pellegrino La Manna and David Hermann Lamparelli

Received: 26 October 2023
Revised: 1 December 2023
Accepted: 4 December 2023
Published: 5 December 2023

1. Introduction

Nitrogen oxides (NO_x) are pollutants introduced into the environment during fossil fuel combustion in automobiles and various non-road vehicles (such as construction equipment, boats, etc.) [1]. NO_x is also emitted from industrial sources such as power plants, boilers, cement kilns, and turbines. NO_x is a common term comprising a mixture of N_2O (a potent greenhouse gas with 300 times more atmospheric warming effect than CO_2), NO, NO_2, N_2O_3, and NO [2]. All these are formed from molecular nitrogen in the air and nitrogen contained in fossil fuels during combustion at high temperatures [3,4]. NO_x emissions constitute environmental and health hazards, facilitating the depletion of the ozone layer and the formation of acid rain, haze, and photochemical smog [3]. Hence, many countries have introduced increasingly stringent regulations and policies on air pollution to reduce NO_x emissions.

As part of these measures and enforced actions, reducing emissions directly by creating and optimizing low-NO_x-formation combustion processes is one strategy. Other techniques, including combustion chambers with lower NO_x formation, have also been developed [5]. Different approaches to reducing NO_x formation include removing nitrogen from flue gas (denitrification), recycling flue gas, and altering combustion parameters [6]. However, the NO_x generated after applying such methods is still beyond the allowed threshold limit. Thus, further advanced technologies have been developed to reduce NO_x emissions effectively. Among the most widely adopted technologies are three-way catalysts [7], NO_x storage, selective non-catalytic reduction (SNCR), and selective catalytic reduction (SCR) using a reducing agent such as ammonia to reduce NO_x to N_2 gas [8]. SCR is characterized by using a catalyst that achieves high levels of conversion of NO_x into N_2 and H_2O at lower temperatures when compared with alternative technologies [6].

In this context, different materials have been used as catalysts for SCR. For example, metal oxides have been used as catalysts, such as vanadium and titanium oxides supported on tungsten, molybdenum, and other elements [6]. For instance, V_2O_5-$WO_3(MoO_3)/TiO_2$ has been used as a commercially effective catalyst. However, the major constraints in the application of this material are the hazardous nature of V_2O_5, the temperature range (300–400 °C), and the side reaction activity towards the oxidation of SO_2. Depending on the application, catalysts that work at lower temperatures are required. Generally, metal-based catalysts work best at temperatures between 232 and 427 °C [6]. In applications that require even lower temperatures, between 177 and 288 °C, platinum and palladium are the best options.

On the other hand, to apply SCR under harsh conditions, zeolite-based catalysts ion-exchanged with Cu or Fe are an appealing, practical alternative for reducing NO_x to molecular nitrogen. Cu-exchanged zeolites have proven effective catalysts for the SCR process [9–13]. The hydrothermal stability of these zeolites is related to their pore size. For instance, zeolites with medium and large pore sizes (such as Cu-ZSM-5, Cu-BEA, and Cu-Y) tend to be less stable, while zeolites with small pore sizes (such as SSZ-13 and SAPO-34) have higher thermal stability and catalytic activity [14]. This stability difference, related to pore size, is connected to the fact that, compared to small pore-sized zeolites, the porous geometry of medium and large pore-sized zeolites is more susceptible to collapse, with a consequent decrease in their surface area and the sintering of surface catalytic active sites.

Although the SAPO-34 and SSZ-13 materials are examples of small pore-sized zeolites with the same structure (CHA topology), the composition difference results in different catalytic performances in the SCR reaction. For instance, Brønsted acid sites in SSZ-13 are related to the aluminum content in the framework. In contrast, the Brønsted site in SAPO-34 is controlled by introducing Si to the $AlPO_4$-34 structure [15], as the introduction of Si at a higher concentration causes the formation of isolated pure Si structures that hold no acidity. Accordingly, controlling the acidity of SAPO-34 is more difficult than its counterpart, SSZ-13. Moreover, the form, location, and concentration of the copper (Cu) in the CHA structure generally plays a crucial role in the catalytic performance in NO_x SCR catalysis. The Cu might exist as isolated Cu^{2+} in the CHA structure, which is the active form in most cases, or as copper oxides (Cu_xO_{x-1}) [16]. Even though SSZ-13 and SAPO-34 are structurally similar, the role of each form of Cu^{2+} and CuO is different. Yu et al. confirmed, by using electron paramagnetic resonance (EPR), that Cu^{2+} was the active form of copper in SAPO-34 [17]. Conversely, in a similar study, it was found that both isolated Cu^{2+} and CuO were the significant actors in contributing to the catalytic activity of Cu/SAPO-34 [18]. However, it was further found that CuO species were more active at lower temperatures while the isolated Cu^{2+} species were preferentially active at higher temperatures [19]. This indicates that it is not only the material's intrinsic composition that controls which form of Cu is present in SAPO-34 but also the condition under which the material works.

Additionally, apart from the Cu distribution and its chemical forms, inherent zeolite composition, such as the Si/Al ratio, affects the hydrothermal stability of the materials. For example, the low Si/Al ratio of CHA improved the material's stability and the widespread

distribution of Cu^{2+} over the material, making ammonia more reactive, enhancing the NO_x SCR activity [13]. Therefore, the Si/Al ratio in the material influences the distribution and concentration of Cu species, their forms, and their locations in the CHA structure. At a lower concentration of Cu, isolated Cu^{2+} might be in the six-member ring and function as an active site, while at a higher concentration, the Cu^{2+} ions agglomerate to form CuO and exist in the eight-member ring. However, in SAPO-34, it has been found that both Cu^{2+} and CuO coexisted even at lower concentrations of Cu loading. A higher Si/Al ratio gave rise to a higher concentration of Al sites in the six-member ring (6 MR). In comparison, with a lower Si/Al ratio, it is unlikely for the material to acquire two Al sites ready to be compensated by the Cu^{2+} [20]. Consequently, Cu^{2+} species are located in the 6 MR at a lower Si/Al ratio and in the 8 MR at a higher Si/Al ratio. Additionally, the chemical form in which Cu exists in the CHA framework also depends on the technique followed during Cu loading. Several approaches can be used to incorporate Cu into the structure of a zeolite, such as ion exchange, solid-state ion exchange, vapor deposition, wet mixing, impregnation, and in situ incorporation within the organic structure-directing agents. Among all of the methods mentioned, the ion exchange was the most effective approach for forming isolated Cu^{2+} in CHA zeolite's structural framework.

Cu-CHA zeolites have been used as an efficient catalyst for NO_x reduction at temperatures higher than 200 °C. However, the major bottleneck in using CHA zeolite is the cost required to synthesize the CHA structures, which mainly revolves around using expensive organic structure-directing agents (OSDAs) [21,22]. Also, the use of OSDAs is accompanied by energy-consuming calcination treatment necessary to completely remove the OSDA molecules from the zeolite structures [23,24]. Therefore, the development of a low-cost, environmentally friendly, and direct methods for synthesizing zeolites free of OSDAs is highly desired.

In this direction, we previously reported a low-cost template-free route for fabricating silicoaluminate CHA zeolite [21]. Here, we report a modified method for the OSDA-free CHA zeolite synthesizing method for the selective catalytic reduction of NO_x. Copper was loaded into the CHA framework under different conditions, and several characterization techniques were employed to reveal the catalyst properties. The chemical and structural composition of the synthesized Cu-CHA zeolites were found promising for NO_x conversion.

2. Materials and Methods

2.1. Synthesis of CHA

The environmentally friendly CHA catalyst was synthesized in accordance with our previous work [25]. The synthesis method involved the addition of an aluminum precursor to an alkaline solution heated at 80 °C. This was followed by the addition of required amounts of ammonium fluoride and silica precursor. Precisely, 4.2 g of KOH (85% pellets, Panreac) was dissolved in deionized water and heated at 80 °C in an oil bath. Then, 3.0 g of aluminum hydroxide (PRS Panreac) was transferred to the alkaline solution while heating at 80 °C and stirred vigorously for 30 min. The solution was allowed to cool to room temperature (RT), after which 1.1 g of ammonium fluoride (ACS reagent, ≥98% Sigma Aldrich, St. Louis, MO, USA) was added. The mixture was further stirred at room temperature for 10 min, followed by the addition of 14.4 g of colloid silica (40 wt%, suspended in water. Aldrich) and allowed to age for 24 h. The final aged gel was then hydrothermally crystallized for 3 days at 160 °C. Finally, the synthesized CHA was separated and washed with plenty of water to decrease the pH to ~7.

2.2. Preparation of Cu-CHA

For the Cu-CHA catalysts, the as-synthesized CHA (K-CHA) was used as the parent material. Before loading Cu onto the framework of CHA zeolites, some of the potassium form of CHA zeolite (K-CHA) was transformed to an ammonium form of CHA zeolite (NH_4-CHA). This was obtained by ion exchange of K-CHA with 1 M of ammonium nitrate

(NH_4NO_3, ≥98% Sigma-Aldrich). For each gram of K-CHA, 30 mL of 1 M NH_4NO_3 was used and heated at 80 °C for two h. The process was repeated with a fresh solution of ammonium nitrate. The aqueous solution ion exchanging technique introduced copper ions over K-CHA and NH_4-CHA zeolites. As the Cu source, $Cu(NO_3)_2 \bullet 3H_2O$ (>99%, Wako) was employed. In a typical synthesis procedure, 1 g of each K-form and NH_4-form of CHA were ion-exchanged with nominal Cu concentrations of 0.05 and 0.1 M. In the procedure, the nominal Cu concentrations were dissolved in deionized water, followed by adding 1 g of each form of as-synthesized CHA powder under continuous stirring at room temperature for 24 h and 80 °C for three h, separately. Then, the solution was centrifuged to separate the products. The obtained solid products were washed, dried overnight at 110 °C, and then calcined at 500 °C (heating rate 10 °C/min) for five h using a muffle furnace. The products were labeled according to the CHA-form and its respective Cu concentration, as well as the temperature at which the product material was synthesized. Thus, that describes how the Cu ion exchange was carried out over the K-form and NH_4-form of the as-synthesized CHA zeolite catalyst. The ion exchange of CHA catalyst with different nominal Cu concentrations is summarized in Table 1.

Table 1. Experimental conditions of the modified Cu-CHA catalysts and relative crystallinity.

S/N	Form of Parent CHA	Name	Conc. (M)	Temperature (°C)	Crystallinity Relative to NH_4-Form (%)	Crystallinity Relative to K-Form (%)
1	NH_4-Form	0.05 Cu-H-CHA	0.05	80	124.96	185.11
2	NH_4-Form	0.1 Cu-H-CHA	0.1	80	108.47	160.68
3	NH_4-Form	0.1 Cu-H-CHA-RT	0.1	25	98.25	145.53
4	K-Form	0.05 Cu-K-CHA	0.05	80	76.03	112.63
5	K-Form	0.1 Cu-K-CHA	0.1	80	79.03	118.37
6	K-Form	0.1 Cu-K-CHA-RT	0.1	25	79.6	117.9

2.3. Characterization Techniques

2.3.1. Structure Study

The parent CHA and copper ion-exchanged CHA (Cu-CHA) zeolite catalysts were characterized by several characterization techniques. To study the catalysts' crystalline phases, X-ray diffraction (XRD) was carried out on a Rigaku Miniflex diffractometer equipped with Cu Kα radiation, λ = 0.15406 nm. The XRD patterns were recorded over 2θ = 5–50° with a scan speed of 3° per min and step size of 0.02°. Nuclear Magnetic Resonance (NMR) spectroscopy was used for molecular identity and structure. The coordination of aluminum of CHA and Cu-CHA zeolites catalysts was investigated using ^{27}Al solid-state Nuclear Magnetic Resonance (MAS NMR) using Varian 500 MHz spectroscopy. The ^{27}Al NMR spectra were acquired via a single pulse experiment with a 30° pulse and a sample spinning frequency of 13 kHz. A combined relaxation delay and acquisition time of 1.1 s was used. A total of 2000 scans were accumulated for each spectrum. External referencing was established using an $Al(NO_3)_3$ solution (0 ppm). The TESCAN instrument was used to conduct elemental and morphology analysis through scanning electron microscopy (SEM) and energy dispersive spectroscopy (EDS) by utilizing secondary electrons.

2.3.2. Acidity Analysis

The acidity of the catalysts was evaluated using temperature-programmed desorption of ammonia (NH_3-TPD) using a BELCAT II Chemisorption analyzer. About 50 mg of a sample was placed in a quartz tube and initially treated at 500 °C for one hour under helium flow. The sample was then ramped to 100 °C and exposed to ammonia blended with helium (10% He) at a 50 mL/min flow rate for 30 min. The sample was then ramped to 600 °C at a ramping rate of 10 °C per minute. The desorbed ammonia was detected by a DTC detector and quantified as a function of temperature.

2.3.3. Surface Area and Pore Volume Distribution

The surface area, pore volumes, and pore size distribution were determined from the N_2 adsorption/desorption isotherm using a Micromeritics ASAP 2020 machine (National Scientific Company Ltd., Jeddah, Saudi Arabia). Firstly, 100 mg of a sample was outgassed at 300 °C for twelve h, and then the analysis was conducted at −195.86 °C in a liquid nitrogen bath. The surface area was calculated by the Brunauer–Emmet–Teller (BET) method, while the pore size distribution was determined using the Horvath–Kawazoe method.

2.3.4. Study of Cu Species in the CHA Structure

The reduction of Cu species was studied by hydrogen temperature-programmed reduction (H_2–TPR) on a Micromeritics Autochem 2910 instrument (National Scientific Company Ltd., Jeddah, Saudi Arabia). Typically, 100 mg of each synthesized catalyst was placed in a U-shaped quartz tube and then preheated at 300 °C for one hour under helium flow. After cooling the sample to 35 °C, the catalyst was heated gradually at 10 °C/min to 850 °C under the flow of 10% H_2 balanced by Ar. The H_2 uptake was measured from the effluent stream using a thermal conductivity detector (TCD). The oxidation states of Cu species were investigated using X-ray photoelectron spectroscopy (XPS) with a scanning X-ray microprobe (Escalab 250, Thermo Fisher Scientific, Waltham, MA, USA) using Al Kα radiation (1486.6 eV). C1s peak with binding energy (BE) of 284.6 eV was used as a standard to calibrate the BE peaks. Prior to the analysis the samples were dispersed in ethanol and then casting on Ta substrate and allowed to evaporate the ethanol.

2.4. Catalytic Evaluation

A fixed-bed reactor made of quartz was used for the catalytic performance evaluation of different series of Cu-CHA catalysts in the NO_x ammonia-selective catalytic reduction (NH_3-SCR) process. Before the evaluation test, 50 mg (40–80 mesh) of a catalyst was mixed with a similar amount of silica gel that was pretreated at 800 °C for 4 h. After that, the combined mixture was heated from room temperature up to 600 °C at a heating rate of 10 °C/min under the flow of oxygen and nitrogen gas (14% O_2/N_2) and held for 30 min as illustrated in Figure 1. Moreover, a gas mixture of 5% H_2O + 14% O_2/N_2 + 5% CO_2 + N_2 was allowed to flow over the sample at the same temperature for two h. Afterward, the reactor was cooled to 120 °C and stabilized for 20 min. Then, a gas feed consisting of 500 ppm NO + 500 ppm NH_3 + 14% O_2/N_2 + 5% CO_2 + 5% H_2O + N_2 was allowed to flow over the catalysts, and the temperature was ramped up to 550 °C at a heating rate of 2.5 °C/min.

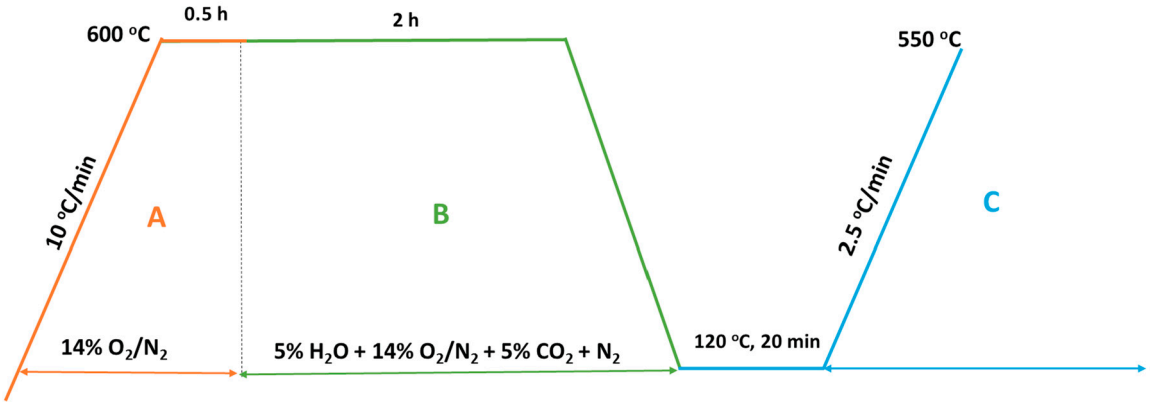

Figure 1. Pre-treatment and reaction procedure. A: pretreatment in 14% O_2/N_2; B: pretreatment in 5% H_2O + 14% O_2/N_2 + 5% CO_2 + N_2 gas mixture; C: temperature-programmed reaction in flow of 500 ppm NO + 500 ppm NH_3 + 14% O_2/N_2 + 5% CO_2 + 5% H_2O + N_2.

3. Results and Discussion

3.1. Structure Study

The crystalline phases and structure of the parent CHA zeolite and Cu-modified CHA zeolites at different conditions were studied using XRD and ^{27}Al NMR, respectively. The XRD patterns shown in Figure 2 revealed that all the as-synthesized CHA zeolites featured diffractograms identical to the well-known XRD patterns of the CHA framework [26], indicating that the as-synthesized CHA zeolites were successfully fabricated. After the ion exchange with ammonium nitrate (NH_4-CHA) and potassium (K-CHA), the XRD patterns remained unchanged, as evidenced by the fact that no new diffractogram peaks or changes were observed and, therefore, the fingerprint of the CHA structure with enhanced peak intensities was maintained during the ion exchange. Generally, loading the Cu to the CHA zeolite in both forms enhanced the relative crystallinity with a noticeable enhancement when the loading was carried on the ammonium form (NH_4-CHA), as presented in Table 1. However, although Cu was loaded onto both the K-CHA and NH_4-CHA zeolite forms, the XRD diffraction patterns of their Cu-modified forms still corresponded mainly to the single K-CHA and NH_4-CHA zeolite phases. This is likely related to the lower loadings of Cu onto the zeolite forms.

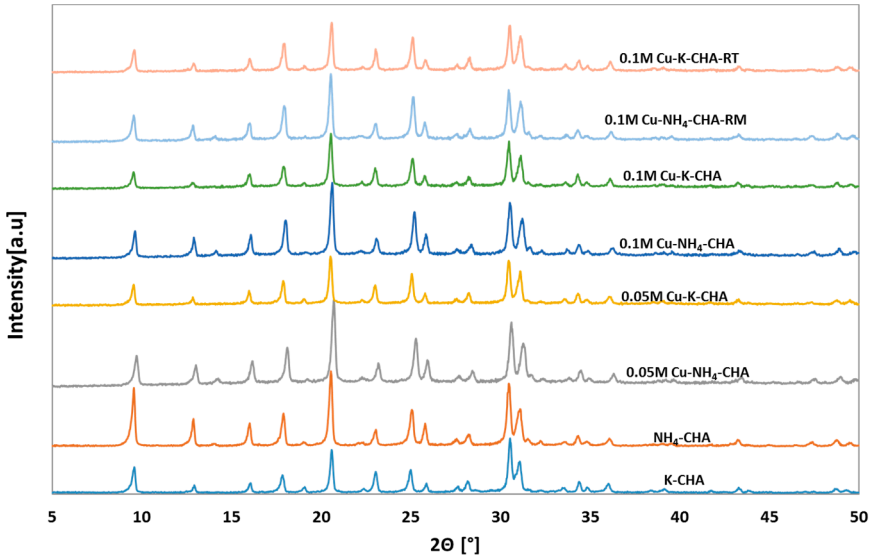

Figure 2. XRD patterns of parent CHA zeolites and CHA zeolite catalysts ion-exchanged with Cu solution at different conditions; K-CHA: CHA as-synthesized, NH_4-CHA: CHA after ion exchange with ammonium nitrate.

For studying the distribution of aluminum in the CHA structure, ^{27}Al NMR was used. As XRD could not give an account of and indications where Al was located in the structure of all the synthesized zeolite forms, the coordination of aluminum can be determined by the ^{27}Al NMR spectrum, which has signals at a chemical shift of ca. 50–60 ppm and ca. 0 ppm for tetrahedral and octahedral coordination, respectively [27–29]. In an attempt to understand the zeolite structure–activity relationship, the location of aluminum atoms in the catalyst framework, the nature or specificity of aluminum bonding in the framework, the closeness of Al framework sites, and the distribution and structure of Al species in non-framework structures are critical factors [30]. In addition, the overall reactivity and activity of the zeolite catalyst may also be influenced by the closeness of framework and non-framework of Al species. Accordingly, in a typical zeolite structural analysis, ^{27}Al NMR excitation is used to probe the distribution of Al atoms between framework and non-framework sites in zeolite catalysts. Figure 3 shows the ^{27}Al NMR spectra of all Cu-CHA catalysts in this context. The Cu-CHA catalysts that were ion-exchanged in the ammonium form showed the presence of tetrahedrally coordinated framework Al at bridging acid

sites in contrast to non-framework octahedrally coordinated Al at the integrated areas of the ~56 and 0 ppm spectral peaks, respectively. A similar result was also observed and reported in the literature [31]. A main spectrum around 56 ppm has been attributed to the tetrahedral coordination of aluminum, while a small peak of ~0 ppm in all the samples designating the presence of an extra framework of aluminum assumed to be non-framework octahedrally coordinated Al in the zeolite structural configuration [32]. The presence of an extra framework in NH_4-form zeolite catalysts resulted from dealumination, which occurred during ion exchange with ammonium ions from the ammonium nitrate solution, as earlier reported in the literature [25]. On the other hand, a different scenario was observed with the K-form of CHA zeolite, as only one peak was observed at ca. 56 ppm, corresponding to the tetrahedral coordination of aluminum in the zeolite catalysts.

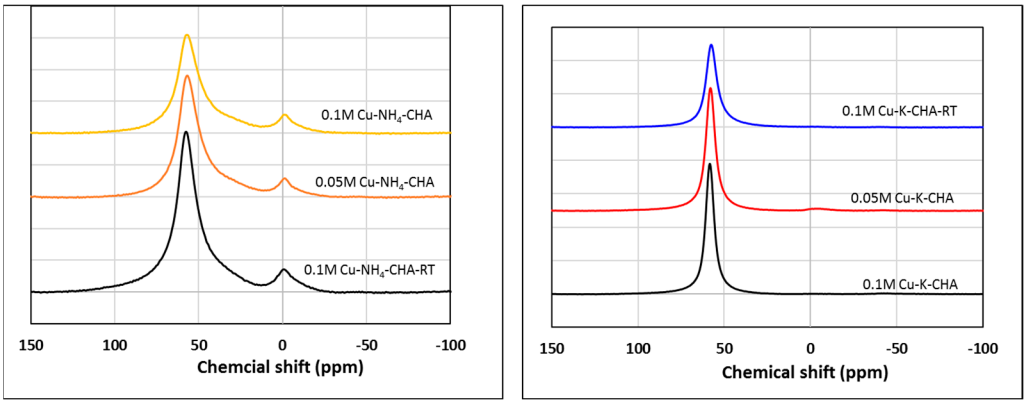

Figure 3. ^{27}Al NMR spectrum of CHA zeolite catalysts ion-exchanged with Cu at different conditions.

3.2. Morphology and Physical Properties

Figure 4 reveals the morphology of the Cu-CHA catalysts prepared at different Cu concentrations and different temperatures. The FE-SEM images presented in Figure 4 have again confirmed the shape and particle size of the catalysts with reference to the OSDA-free CHA zeolite reported previously [25]. In principle, the particles are cuboids in shape and submicron in size. These cuboids were agglomerated and formed larger particles with sizes ranging from 5–8 µm. It was observed that the modifications to the parent CHA zeolite did not alter the morphology of the Cu-CHA zeolite catalysts. The loading of Cu to the CHA structure was confirmed by the elemental distribution map (EDS/EDX), as presented in Figure 5 and Table 2.

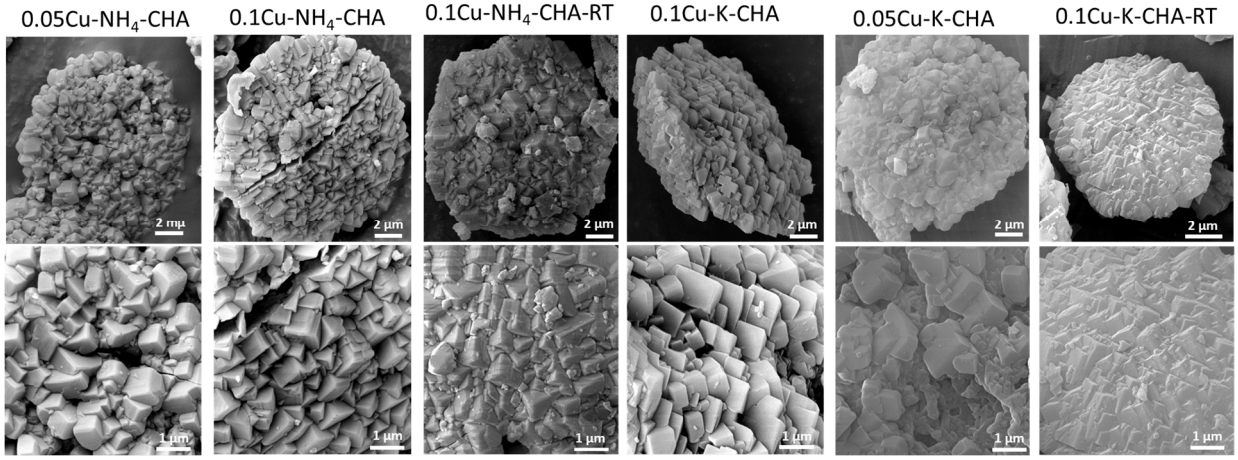

Figure 4. FE-SEM images of CHA zeolites catalysts ion-exchanged with Cu solution at different conditions.

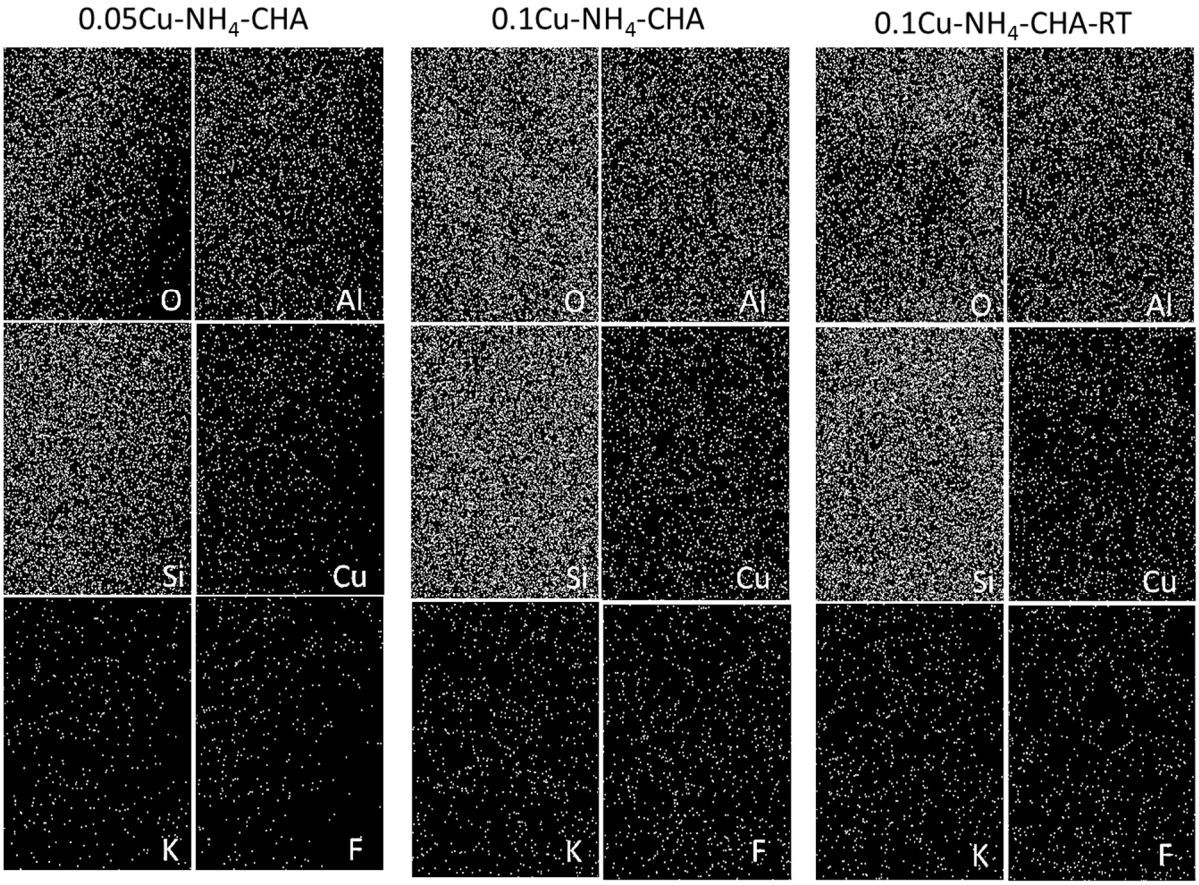

Figure 5. Elemental distribution map (SEM/EDS) of Cu-CHA catalysts prepared from NH_4-CHA.

Table 2. Surface area and pore volume distribution of a series of Cu-CHA catalysts.

Sample	Surface Area (m^2/g)				Pore Volume (cm^3/g)			Cu/Al *
	S_{ext}	S_{micro}	$S_{tot.}$	S_L	V_{micro}	V_{meso}	V_{tot}	
0.05 M Cu-NH_4-CHA	20	409	429	465	0.150	0.024	0.174	0.72
0.1 M Cu-NH_4-CHA	21	422	443	482	0.155	0.025	0.180	0.81
0.1 M Cu-NH_4-CHA-RT	13	457	470	498	0.167	0.018	0.185	0.66
0.05 M Cu-K-CHA	29	158	186	240	0.060	0.037	0.098	-
0.1 M Cu-K-CHA	23	296	319	364	0.112	0.033	0.145	-
0.1 M Cu-K-CHA-RT	6	63	69	90	0.024	0.023	0.047	-

* Elemental analysis was conducted using EDX.

The textural properties of as-synthesized catalysts were determined by the N_2 adsorption/desorption method. Figure 6 shows the N_2 adsorption/desorption isotherms of the Cu-exchanged zeolites and their corresponding pore width distributions against the differential volumes using the Horvath–Kawazoe model. The numerical treatment of N_2 isotherms provides surface area and pore volume presented in Table 2. Remarkably, the isotherms of the NH_4-CHA zeolite type catalysts exhibited higher uptake of N_2 than the K-Form of zeolite catalysts. The poor N_2 uptake by the Cu-CHA catalysts prepared from the K-Form of CHA highlights the importance of pore openings of CHA, which were blocked by potassium ions prior to any modifications. The previous N_2 analysis showed no adsorption/desorption for the K-CHA [25]. However, an increase in ion exchange temperature from room temperature (RT) to 80 °C enhanced the degree of potassium exchange with Cu, as indicated by an increase in the BET surface area and pore volume, Table 2. The

higher ion-exchange temperature facilitated the ion-exchange process even when the Cu concentration was 0.05 M.

Noticeably, both the NH_4-CHA and K-CHA forms of the zeolite synthesized catalysts exhibit a sharp increase in the relative pressure below 0.01, indicating the abundant presence of micropores [11]. However, as seen in Figure 6, all the K-CHA forms of zeolite samples exhibit a mixed type 1 and type IV isotherm with an H1 type hysteresis loop in the range of $P/P^0 > 0.8$, indicating the representation of dominant mesoporosity with only a small contribution from macroporosity [33]. Similarly, based on the pore size distribution curves and SEM images, it can be inferred that the mesoporous structure was predominantly formed between cuboid crystal particles of all the as-synthesized zeolite catalysts. Therefore, considering the surface area and pore volume of the as-synthesized zeolite catalysts, it can be inferred that their textural properties are highly similar to those of the conventional SAPO-34 and SSZ-13 zeolites. Thus, the synthesis procedure adopted is promising.

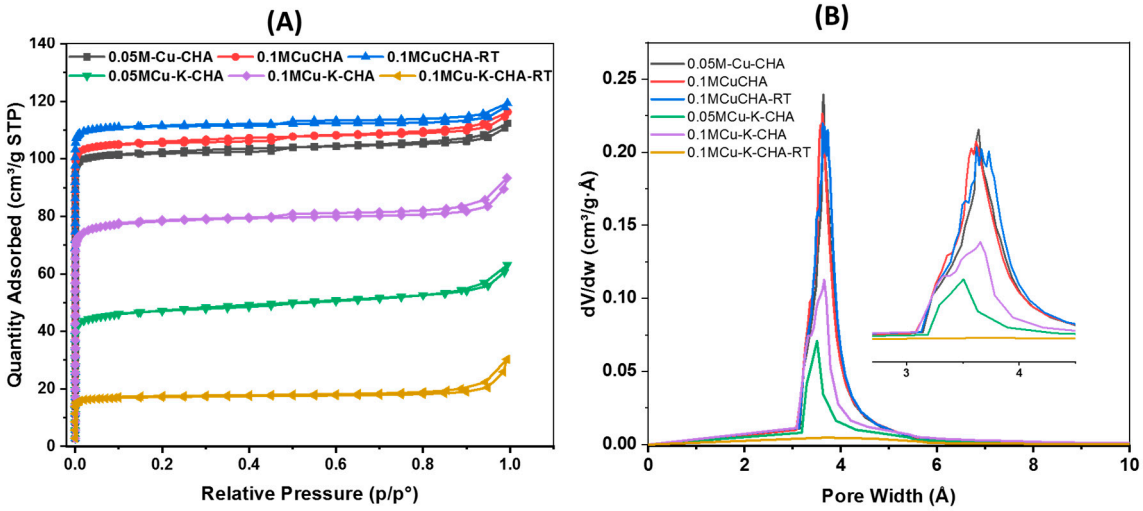

Figure 6. N_2 adsorption/desorption isotherms of Cu-CHA zeolites treated under different conditions (**A**) and the pore width distribution using the Horvath–Kawazoe method (**B**).

The acidity of the as-synthesized catalysts was evaluated using the NH_3-TPD to correlate the different types of ion exchanges to the active sites of the catalysts. The NH_3-TPD profiles are presented in Figure 7, linking the form of the CHA used and the ion-exchange conditions. The NH_3-TPD is the most appropriate method for quickly determining the acidic properties of solids acid materials [34], as it conveniently describes total acidity, strength, and distribution from peak area, position, and shape, respectively. However, in this study, attention is concentrated on the strength of the acid sites in the as-synthesized zeolite catalysts, which is determined by the relative position of the NH_3 desorption peaks in the NH_3-TPD curves. In the literature, the desorption profile of NH_3 from zeolite catalysts, particularly Cu ion-exchanged CHA forms of zeolites, typically has three commonly known peaks [35–38], namely, a low-temperature peak below 200 °C; an intermediate-temperature peak at a range between 250 and 350 °C; and a high-temperature peak at 400–500 °C. Accordingly, the low-temperature peak is assigned to NH_3 desorption from Lewis acid sites. In contrast, the intermediate-temperature peak is characteristic of Cu-sites, and the high-temperature rise is ascribed to Brønsted acid sites. The ammonia desorption profiles presented in Figure 7, along with their deconvolution in Figures S4–S9, demonstrate that all catalysts have three levels of acid sites. However, catalysts prepared using the NH_4-form of Cu-CHA zeolites have a higher acid density than those prepared using the K-form of Cu-CHA zeolites, as presented in Table S1. This increase in acid density is due to the removal of potassium ions during the ion exchange process with ammonium nitrate. The N_2 adsorption/desorption isotherms confirm that the pores of K-form of CHA zeolites were blocked, which limits accessibility to acidic sites. Consequently, this has elucidated

the difference in the strength of the acid sites in the two forms of the as-synthesized zeolite catalysts, which correlates to their different NH_3-SCR activity.

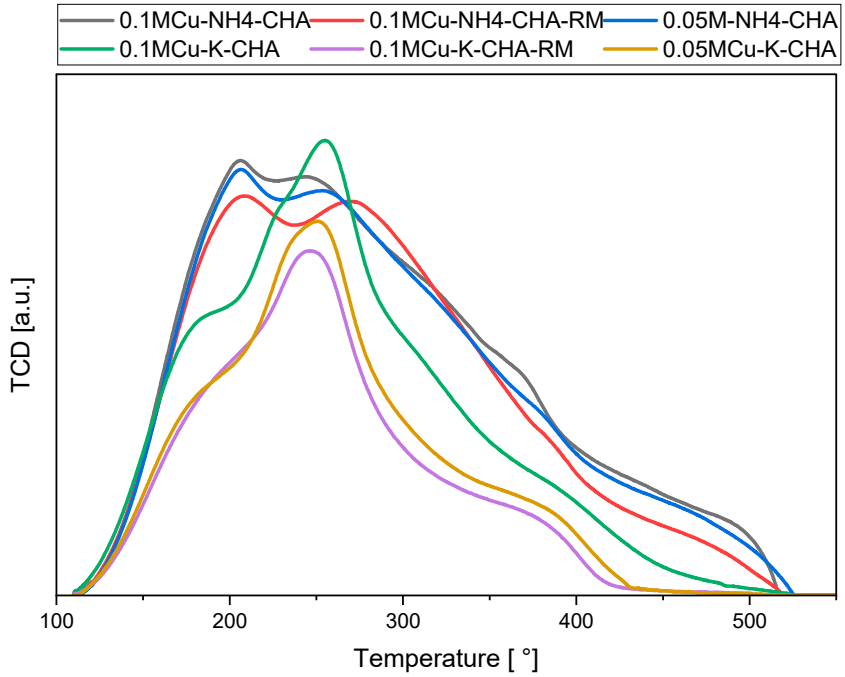

Figure 7. NH_3-TPD profile CHA zeolite catalysts ion-exchanged at different conditions.

3.3. Cu Loading to CHA Structure

In this work, H_2-TPR experiments were carried out on the NH_4-form and K-form of Cu ion-exchanged CHA zeolite catalysts. Figure 8 presents the H_2-TPR profiles of Cu-CHA catalysts under different conditions. The H_2-TPR profile of the Cu-CHA ion exchanged catalyst over the NH_4-form showed a broad low-temperature peak centered around 250 °C. The deconvolution of this peak into three peaks is shown in Figures S1–S3 (see the supporting information). The first peak is ascribed to the reduction of isolated Cu^{2+} to Cu^{+}, while the second and third peaks are associated with the reduction of CuO to Cu^0 and Cu^{+} to Cu^0, respectively [12,39–41]. Therefore, the catalysts are characterized by the presence of Cu^0 and Cu^{+} species independent of Cu loading. The intensities of each peak depend on the Cu concentration and the ion exchange temperature. The 0.1 MCu-NH_4-CHA catalyst showed the highest peak intensity, followed by 0.05 Cu-NH_4-CHA and 0.1 MCu-NH_4-RT catalysts. However, two other peaks are visible at 650 °C and 800 °C, belonging to the reduction of highly stable Cu^{+}, a characteristic of the CHA framework [42]. Accordingly, the main consideration is that the high-reduction peaks are denoted by the reduction of Cu^{+} to Cu^0.

The catalysts developed from the K-form of the CHA showed well-defined low-temperature peaks centered around 240 °C, which are ascribed to the reduction of the $Cu^{II}OH$ species [10,43,44]. Similarly, as seen from their H_2-TPR, other well-defined peaks assigned to Cu^{II} species [10,43,44] are apparent at about 364 °C.

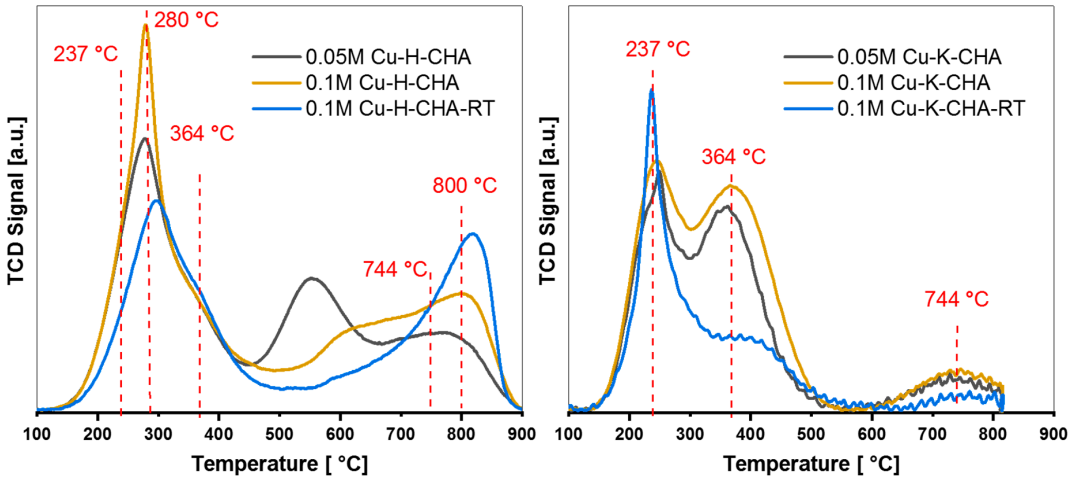

Figure 8. H_2-TPR profile of CHA zeolite catalysts ion-exchanged under different conditions.

Information about the oxidation or chemical state of Cu species on the different NH_4-form CHA catalyst surfaces and their distribution was probed by XPS. It is worth mentioning that copper XPS analysis should be carried out carefully as copper is highly sensitive to radiation [45]. The exposure of X-ray radiation can lead to the reduction of Cu species to Cu^+. Therefore, for copper XPS analysis, sample freezing, minimizing exposure time, using a monochromatized X-ray source, or a low energy X-ray source are recommended. However, integration of H_2-TPR and XPS analysis would conveniently explain the presence of the type of Cu species in a sample. Figure 9 shows the XPS spectra of Cu species before and after ion etching the samples for 30 s. All catalysts exhibited the presence of the same Cu species but with different peak intensities due to variations in Cu concentrations and ion exchange temperature. The XPS profile confirmed the presence of Cu 2p3/2 at lower binding energy ca. 932 and 933 eV belonging to Cu^+ and Cu^{2+}, respectively. Cu 2p1/2 was located at higher binding energy around 952 and 953 eV, features indicating that Cu existed primarily in the as-synthesized catalysts as Cu^+ and Cu^{2+}, respectively [46]. The Shakeup peaks, a property of the dispersed Cu^{2+}, were also observed at binding energies between 942 to 943 eV. Similarly, weak satellite features around 940 and 960 eV are generally assigned to Cu^{2+} in the CuO phase [47,48].

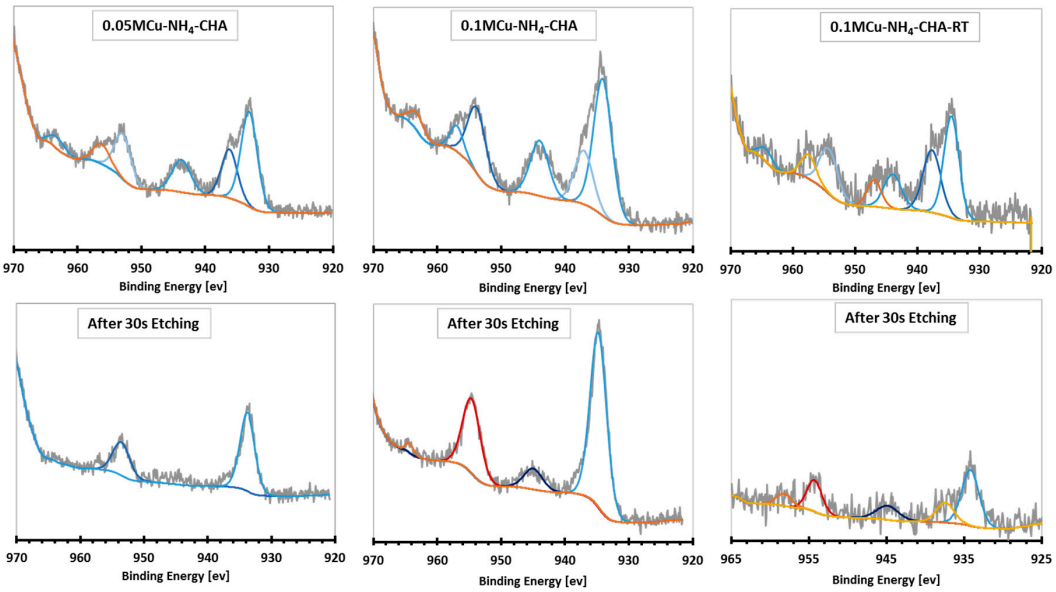

Figure 9. The XPS spectra of Cu species before and after etching of the NH_4-form of CHA zeolite catalysts with different Cu loading.

Concerning ion-etched samples, it was observed that the intensities of all the satellite peaks that appeared in the as-synthesized zeolite catalysts were drastically reduced, and some even disappeared. Still, the Cu 2p1/2 and 2p3/2 peaks of 0.1 M Cu-NH_4-CHA emerged sharply at their standard positions. The disappearance of those peaks means that their assigned Cu species were removed, and the analysis reached close to the surface of the as-synthesized zeolite catalyst. This finding points to preferential dealumination close to the surface of the 0.05 M Cu-NH_4-CHA and 0.1 M Cu-NH_4-CHA-RT, presumably caused by diffusion limitations experienced by the Cu ions in those mentioned catalysts. By implication, since framework Al is related initially to acid sites, dealumination in those catalysts caused a decrease in their acid sites. Hence, this suggests that Cu species within the zeolite catalyst 0.1 M Cu-NH_4-CHA were well distributed and stabilized and may not be significantly affected by the working conditions, such as operating temperature, and by the other reactive species present inside the catalyst's microporous structure.

This reveals that ion-etching created contrast between the as-synthesized catalysts through differences in the topographical nature of Cu species distribution on the surface and within the microstructures of the catalysts. In addition, the etching process exposed the supposedly catalytic active sites on the surface of the modified and Cu ion-exchanged CHA zeolite catalysts. Because the impact of the etching technique unveiled the stability of seemingly active sites, it could help understand the relationship between the surface structure of the catalysts and their catalytic performance in NO_x conversion.

3.4. Catalytic Evaluation

In NH_3-SCR tests using the as-synthesized zeolite catalysts, Figures 10 and 11 depict NO_x conversions as a function of the reaction temperatures ranging between 120 and 550 °C. As can be seen, the NO_x conversion rose with temperature as the NH_3-SCR process was initiated, reached a maximum, and then declined. This is particularly noticeable in the results manifested by 0.05 MCu-NH_4-CHA and 0.1 MCu-NH_4-CHA-RT, which perhaps is associated with their inherent structural and catalytic characteristics that are, to a certain extent, different from the 0.1 M Cu-NH_4-CHA.

Among the synthesized catalysts, 0.1 MCu-NH_4-CHA exhibited the best catalytic performance for NO_x conversion. The catalyst showed 100% conversion with steady thermal stability over a wide range of higher reaction temperatures between ca. 261 and 520 °C. Interestingly, this zeolite catalyst achieved 50% NO_x conversion at 192 °C and reached complete 100% NO_x conversion at temperatures from 261 °C. This result reveals a significant catalytic improvement compared to the conventional Cu-based chabazite (Cu-CHA) catalysts, whose NO_x conversion efficiency is relatively low at temperatures below 200 °C. Thus, NO_x must first be stored over conventional zeolite catalysts and converted at higher temperatures [49]. In addition, while the local Cu/Al ratio varied among the samples, the 0.1 M Cu-NH_4-CHA is the material that has the highest Cu/Al ratio and, much more likely, will have a higher Si/Al ratio, too. It has been generally considered that samples with a higher Si/Al ratio are thermally stable [50,51]. It is known that the thermal stability of Cu ion-exchanged zeolite-based catalysts also depends on the Cu/Al ratio [50], as confirmed by this study's results (Table 2). Therefore, it can be speculated that the enhancement of the overall thermal stability of 0.1 M Cu-NH_4-CHA over a wide temperature range during NO_x conversion could be attributed to the higher Cu/Al ratio. Furthermore, the abundance of stable Cu species, particularly Cu^{2+} in the framework of Cu-based CHA zeolite catalysts, is responsible for better NO_x conversion during NH_3-SCR [52]. To further support this point, it was indicated that different Cu active site locations were the reason why Cu-based zeolite catalysts exhibited different catalytic activity profiles [9,43,53]. Therefore, as Cu^{2+} species are well distributed and stabilized within 0.1 M Cu-NH_4-CHA, as shown in the XPS profile of the ion-etched sample in Figure 9; thus, 0.1 M Cu-NH_4-CHA displayed the best catalytic performance relative to 0.05 M Cu-NH_4-CHA and 0.1 M Cu-NH_4-CHA-RT over a wider operating temperature range.

It is essential to point out that the NO_x conversion efficiency of 0.1 MCu-NH_4-CHA zeolite catalyst presents a promising result, as its NO_x conversion index outperformed the earlier reported Cu-CHA zeolite catalysts, which achieved 100% NO_x conversion only at temperatures from 220 to 380 °C [52]. Similarly, Cu-based zeolite catalysts mainly showed high NH_3-SCR activity in the temperature window of 350–550 °C, where Cu-ZSM-5, Cu-SSZ-13, and Cu-BEA showed maximum NO_x conversion at temperatures of 425, 450, and 550 °C, respectively [53]. In another similar study, ion-exchanged Cu-based SSZ-13 catalysts achieved approximately 80% NO_x conversion at temperatures between 175 and 400 °C [54]. Furthermore, the NO_x conversion rate of V-based catalysts with Sb remained at 80% at temperatures between 270 and 450 °C [55], far below the catalytic performance of 0.1 MCu-NH_4-CHA reported in this study. This study, therefore, clearly shows that the NO_x catalytic performance of 0.1 M Cu-NH_4-CHA is superior to similar and other $DeNO_x$ catalysts, as indicated above. Hence, the result presented by 0.1 M Cu-NH_4-CHA proffers a solution towards achieving more effective use of Cu-CHA catalysts in maximizing NO_x conversion strategies for abatement of NO_x and pollution-free urban atmospheres.

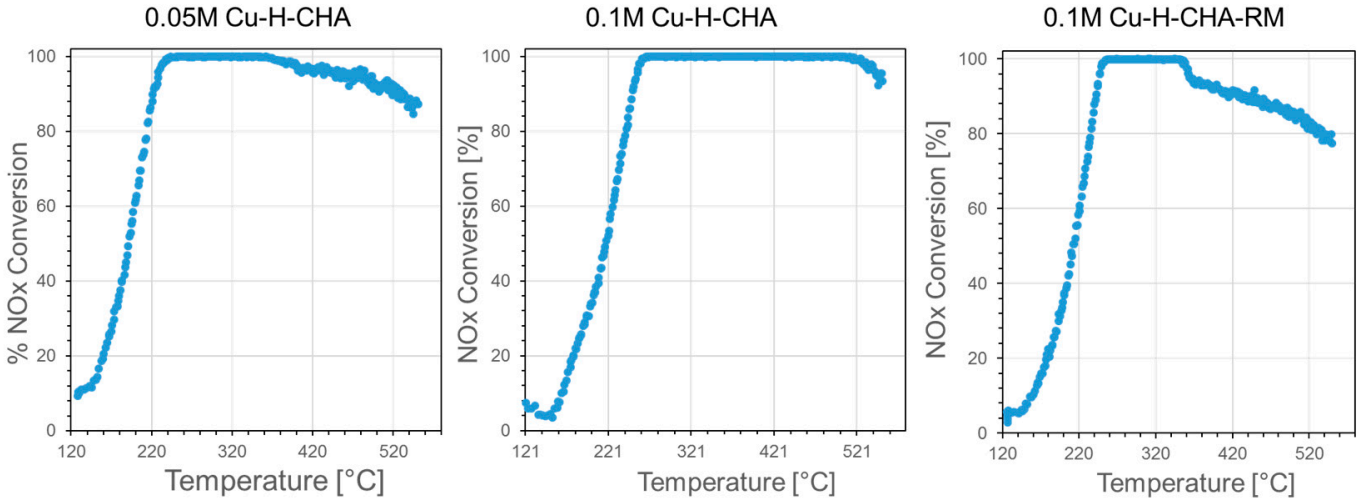

Figure 10. NO_x conversion by the NH_4-CHA zeolite catalyst ion-exchanged at different concentrations and temperatures. Catalyst loading: 50 mg (40–80 mesh) mixed with 50 mg silica gel. Reaction conditions: 500 ppm NO + 500 ppm NH_3 + 14% O_2/N_2 + 5% CO_2 + 5% H_2O + N_2. Total gas flow rate: 200 mL/min. Space velocity 240 L/h-g. Temperature ramp: 2.5 °C/min. Total reaction time: 172 min.

Similar catalytic behavior was observed between NH_4-CHA and K-CHA forms of the as-synthesized zeolite catalysts. Although, as seen in Figure 11, the NO_x conversion also increased with temperature, the catalytic NO_x conversion efficiency exhibited by the K-CHA forms of zeolite catalysts was unsatisfactory. Their conversion profiles were also not maintained over a wide range of temperatures. Instead, it suddenly declined. This indicates that the catalysts were thermally unstable, and as a result, the catalysts suffered a decrease in NO_x conversion even at temperatures far below 400 °C. At ca. 330 °C, the K-CHA form zeolite catalysts achieved <80%, 40%, and ca. 68% NO_x conversion for 0.05 MCu-K-CHA, 0.1 M Cu-K-CHA, and 0.1 M Cu-K-CHA-RT, respectively. Immediately after attaining these apex conversions, the conversions dropped drastically due to deactivation. The observed deactivation may be attributed to surface modifications caused by potassium (K) masking or poisoning, as alkali metals (Na, K) and alkali earth-metals (Mg, Ca) are documented as poisons for SCR catalysts [56]. In this case, the potassium (K) masking or poisoning effect might be responsible for reducing the surface active sites of the K-CHA catalysts or initiating the transformation of isolated Cu ions to $Cu_xO_y/Cu^{II}OH$ clusters, respectively. The masking effect of K is usually caused by its ions anchoring to Brønsted acid sites because K has more affinity for Brønsted acid sites than isolated Cu ions or

directly supplanting Cu ions due to strong difference in electropositivity [57]. On the other hand, the transformation of isolated Cu ions to $Cu_xO_y/Cu^{II}OH$ clusters might be initiated by electronic interaction through which Cu species behave as anions by accepting electrons from K via filled 4s orbitals and partially filled extended 4p orbitals [58]. This demonstrates that the incorporation of K into the catalysts affected the surface active sites or acid sites generated by the incorporation of Cu in the K-CHA zeolite catalysts. Therefore, Cu species, particularly in isolated forms, are inferred to be the active sites in the NH_3-SCR process, in agreement with earlier observations [59]. This can be further supported by the apparent difference in the H_2-TPR profiles, where a blend of isolated Cu^+ and Cu^{2+} dominated the forms of Cu species in Cu-NH_4-CHA zeolite catalysts. At the same time, $Cu^{II}OH$ was the characteristic principal species in the Cu-K-CHA catalysts. The manifested difference in $DeNO_x$ catalytic activity between the as-synthesized ion-exchanged Cu-NH_4-CHA and Cu-K-CHA zeolite catalysts finally confirmed this.

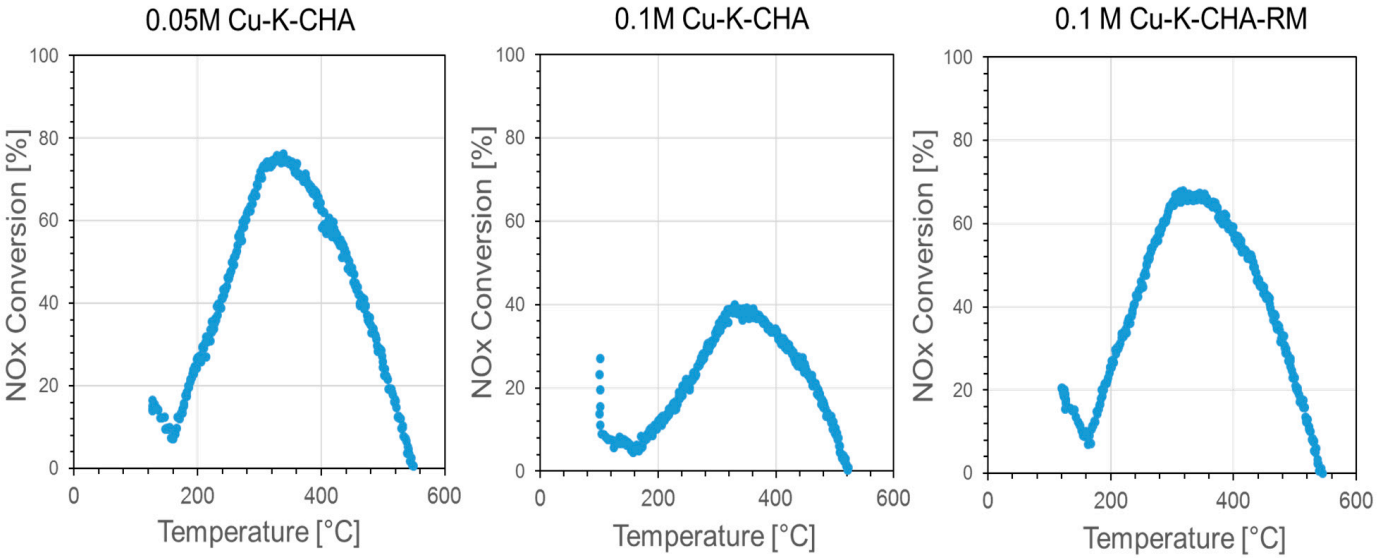

Figure 11. NO_x conversion by the K-CHA zeolite catalyst ion-exchanged at different concentrations and temperatures. Catalyst loading: 50 mg (40–80 mesh) mixed with 50 mg silica gel. Reaction conditions: 500 ppm NO + 500 ppm NH_3 + 14% O_2/N_2 + 5% CO_2 + 5% H_2O + N_2. Total gas flow rate: 200 mL/min. Space velocity 240 L/h-g. Temperature ramp: 2.5 °C/min. Total reaction time: 172 min.

4. Conclusions

Room- and low-temperature Cu ion-exchanged NH_4-forms and K-forms of CHA zeolite catalysts were synthesized with Cu loadings of 0.05 and 0.1 M. All as-synthesized Cu-NH_4-CHA zeolite catalysts showed higher catalytic NO_x conversion than the Cu-K-CHA catalysts. The XRD profile revealed that all the as-synthesized CHA zeolites featured diffractograms identical to the well-known XRD patterns of the CHA framework. The ^{27}Al NMR spectroscopic results indicated that the NH_4-CHA possessed tetrahedral and octahedral aluminum coordination within the zeolite framework. At the same time, the K-CHA form was dominated by the tetrahedral coordination of aluminum. This signifies that NH_4-CHA zeolite catalysts possessed more Al coordination in the extraframework position than in the K-CHA forms.

Morphologically, the NH_4-CHA type formed more bundles of well-interconnected cuboids than the other zeolite-type catalysts, beneficial for keeping them structurally intact and perhaps advantageous to their thermal stability. In terms of textural properties, considering the surface area and pore volume of the as-synthesized zeolite catalysts, it can be inferred that their textural properties are similar to those of the conventional SAPO-34 and SSZ-13 zeolites. Thus, the synthesis procedure adopted is promising. The Cu

ion-exchanged CHA forms of zeolites typically have three commonly known acid sites: Lewis sites, Cu-sites, and Brønsted sites. In this context, the prepared Cu ion-exchanged NH_4-form of CHA zeolites showed mainly two acid sites characterized by Lewis and Cu-sites. In contrast, the K-Form of Cu-CHA zeolite catalysts were characterized by only Cu-sites and, thus, supported the notion that their NH_3-SCR activity for NO_x conversion is undoubtedly dissimilar.

The H_2-TPR profile of the Cu-NH_4-CHA proved that the Cu species distribution over the catalysts was dominated by a mixture of Cu^+ and Cu^{2+} species, while in the other CHA zeolite catalysts, the predominant Cu species were mainly Cu in the form of $Cu^{II}OH$. The XPS spectra of Cu-NH_4-CHA further supported this: that Cu existed primarily in the catalysts as Cu^+ and Cu^{2+}.

To reveal this study's most important finding, the as-synthesized Cu-NH_4-CHA zeolite catalysts, particularly 0.1 M Cu-NH_4-CHA, achieved superior performance in the NH_3-SCR reaction with 100% NO_x conversion within the temperature window between 192 and 261 °C. This seems to be one of the lowest temperature windows compared to the windows of NH_3-SCR reaction for NO_x conversions by Cu-zeolites-based catalysts reported in the literature. In contrast to the Cu-NH_4-CHA, the as-synthesized Cu-K-CHA zeolite catalysts suffered significantly from the potassium (K) poisoning effect, causing notable deactivation accompanied by the rapid loss of NH_3-SCR catalytic activity.

Finally, this work shows that Cu-based CHA zeolite, particularly the NH_4-CHA forms, can be synthesized successfully without using an organic structure-directing agent (OSDA) with desired morphology; texture; and framework Al coordination, which are key factors for determining the structure–activity relationship in zeolite catalytic reactions. Thus, this synthesis technique can be directed towards actual application for their synthesis and utilization in $DeNO_X$ catalytic strategies.

Supplementary Materials: The following supporting information can be downloaded at: https://www.mdpi.com/article/10.3390/app132413001/s1, Figure S1: Deconvolution of the H2-TPD profile of 0.1 M Cu-H-CHA catalyst; Figure S2: Deconvolution of the H2-TPD profile of 0.05 M Cu-H-CHA catalyst; Figure S3: Deconvolution of the H2-TPD profile of 0.1 M Cu-NH_3-CHA catalyst; Figure S4: NH_3-TPD deconvolution of 0.1 M Cu-NH_4-CHA catalyst; Figure S5: NH_3-TPD deconvolution of 0.1 M Cu-NH_4-CHA-RM catalyst; Figure S6: NH_3-TPD deconvolution of 0.05 M-NH_4-CHA catalyst; Figure S7: NH_3-TPD deconvolution of 0.1 M Cu-K-CHA catalyst; Figure S8: NH_3-TPD deconvolution of 0.1 M Cu-K-CHA-RM catalyst; Figure S9: NH_3-TPD deconvolution of 0.05 M-NH_4-CHA catalyst; Table S1: Amount of weak, medium, and strong acid sites.

Author Contributions: Conceptualization, O.M. and Z.H.Y.; methodology, J.W.S., O.M. and H.Z.; validation, J.W.S., M.A.S., H.Z. and E.S.; formal analysis, G.A.N., A.I.B., H.Z., M.A.S. and E.S.; investigation, G.A.N., A.I.B., H.Z., E.S. and M.A.S.; writing—original draft preparation, G.A.N., H.A., M.A.S., E.S., H.Z. and J.W.S.; writing—review and editing, all authors; supervision, J.W.S., Z.H.Y. and O.M.; project administration, J.W.S. and O.M. All authors have read and agreed to the published version of the manuscript.

Funding: This research received no external funding.

Institutional Review Board Statement: Not applicable.

Informed Consent Statement: Not applicable.

Data Availability Statement: Data is contained within the article.

Conflicts of Interest: The authors declare no conflict of interest.

References

1. Zhao, H.; Hill, A.J.; Ma, L.; Bhat, A.; Jing, G.; Schwank, J.W. Progress and future challenges in passive NO adsorption over Pd/zeolite catalysts. *Catal. Sci. Technol.* **2021**, *11*, 5986–6000. [CrossRef]
2. Cassia, R.; Nocioni, M.; Correa-Aragunde, N.; Lamattina, L. Climate Change and the Impact of Greenhouse Gasses: CO_2 and NO, Friends and Foes of Plant Oxidative Stress. *Front. Plant Sci.* **2018**, *9*, 273. [CrossRef] [PubMed]

3. Boningari, T.; Smirniotis, P.G. Impact of nitrogen oxides on the environment and human health: Mn-based materials for the NOx abatement. *Curr. Opin. Chem. Eng.* **2016**, *13*, 133–141. [CrossRef]
4. ICAC. *Selective Catalytic Reduction (SCR) Control of NOx Emissions from Fossil Fuel-Fired Electric Power Plants*; ICAC: Hong Kong, China, 2009; pp. 1–31.
5. Fontaras, G.; Franco, V.; Dilara, P.; Martini, G.; Manfredi, U. Development and review of Euro 5 passenger car emission factors based on experimental results over various driving cycles. *Sci. Total Environ.* **2014**, *468–469*, 1034–1042. [CrossRef] [PubMed]
6. Gao, F.; Tang, X.; Yi, H.; Zhao, S.; Li, C.; Li, J.; Shi, Y.; Meng, X. A review on selective catalytic reduction of NOx by NH_3 over Mn–based catalysts at low temperatures: Catalysts, mechanisms, kinetics and DFT calculations. *Catalysts* **2017**, *7*, 199. [CrossRef]
7. Wang, J.; Chen, H.; Hu, Z.; Yao, M.; Li, Y. A review on the Pd-based three-way catalyst. *Catal. Rev.-Sci. Eng.* **2015**, *57*, 79–144. [CrossRef]
8. Tang, Q.; Denison, M.; Adams, B.; Brown, D. Towards comprehensive computational fluid dynamics modeling of pyrolysis furnaces with next generation low-NOx burners using finite-rate chemistry. *Proc. Combust. Inst.* **2009**, *32*, 2649–2657. [CrossRef]
9. Kwak, J.H.; Tran, D.; Burton, S.D.; Szanyi, J.; Lee, J.H.; Peden, C.H.F. Effects of hydrothermal aging on NH_3-SCR reaction over Cu/zeolites. *J. Catal.* **2012**, *287*, 203–209. [CrossRef]
10. Gao, F.; Peden, C.H.F. Recent Progress in Atomic-Level Understanding of Cu/SSZ-13 Selective Catalytic Reduction Catalysts. *Catalysts* **2018**, *8*, 140. [CrossRef]
11. Xie, L.; Liu, F.; Ren, L.; Shi, X.; Xiao, F.S.; He, H. Excellent performance of one-pot synthesized Cu-SSZ-13 catalyst for the selective catalytic reduction of NOx with NH_3. *Environ. Sci. Technol.* **2014**, *48*, 566–572. [CrossRef]
12. Torre-Abreu, C.; Ribeiro, M.F.; Henriques, C.; Delahay, G. NO TPD and H2-TPR studies for characterisation of CuMOR catalysts. The role of Si/Al ratio, copper content and cocation. *Appl. Catal. B Environ.* **1997**, *14*, 261–272. [CrossRef]
13. Shan, Y.; Shan, W.; Shi, X.; Du, J.; Yu, Y.; He, H. A comparative study of the activity and hydrothermal stability of Al-rich Cu-SSZ-39 and Cu-SSZ-13. *Appl. Catal. B Environ.* **2020**, *264*, 118511. [CrossRef]
14. Moliner, M.; Martínez, C.; Corma, A. Synthesis strategies for preparing useful small pore zeolites and zeotypes for gas separations and catalysis. *Chem. Mater.* **2014**, *26*, 246–258. [CrossRef]
15. Tan, J.; Liu, Z.; Bao, X.; Liu, X.; Han, X.; He, C.; Zhai, R. Crystallization and Si incorporation mechanisms of SAPO-34. *Microporous Mesoporous Mater.* **2002**, *53*, 97–108. [CrossRef]
16. Deka, U.; Juhin, A.; Eilertsen, E.A.; Emerich, H.; Green, M.A.; Korhonen, S.T.; Weckhuysen, B.M.; Beale, A.M. Confirmation of isolated Cu^{2+} ions in SSZ-13 zeolite as active sites in NH_3-selective catalytic reduction. *J. Phys. Chem. C* **2012**, *116*, 4809–4818. [CrossRef]
17. Yu, T.; Hao, T.; Fan, D.; Wang, J.; Shen, M.; Li, W. Recent NH_3-SCR mechanism research over Cu/SAPO-34 catalyst. *J. Phys. Chem. C* **2014**, *118*, 6565–6575. [CrossRef]
18. Wang, L.; Gaudet, J.R.; Li, W.; Weng, D. Migration of Cu species in Cu/SAPO-34 during hydrothermal aging. *J. Catal.* **2013**, *306*, 68–77. [CrossRef]
19. Lai, S.; Meng, D.; Zhan, W.; Guo, Y.; Guo, Y.; Zhang, Z.; Lu, G. The promotional role of Ce in Cu/ZSM-5 and in situ surface reaction for selective catalytic reduction of NOx with NH_3. *RSC Adv.* **2015**, *5*, 90235–90244. [CrossRef]
20. Fickel, D.W.; Lobo, R.F. Copper coordination in Cu-SSZ-13 and Cu-SSZ-16 investigated by variable-temperature XRD. *J. Phys. Chem. C* **2010**, *114*, 1633–1640. [CrossRef]
21. Dusselier, M.; Davis, M.E. Small-Pore Zeolites: Synthesis and Catalysis. *Chem. Rev.* **2018**, *118*, 5265–5329. [CrossRef] [PubMed]
22. Sachse, A.; García-Martínez, J. Surfactant-Templating of Zeolites: From Design to Application. *Chem. Mater.* **2017**, *29*, 3827–3853. [CrossRef]
23. Vattipalli, V.; Paracha, A.M.; Hu, W.; Chen, H.; Fan, W. Broadening the Scope for Fluoride-Free Synthesis of Siliceous Zeolites. *Angew. Chem. Int. Ed.* **2018**, *57*, 3607–3611. [CrossRef] [PubMed]
24. Zholobenko, V.; Garforth, A.; Dwyer, J. TGA-DTA study on calcination of zeolitic catalysts. *Thermochim. Acta* **1997**, *294*, 39–44. [CrossRef]
25. Nasser, G.A.; Muraza, O.; Nishitoba, T.; Malaibari, Z.; Al-Shammari, T.K.; Yokoi, T. OSDA-free chabazite (CHA) zeolite synthesized in the presence of fluoride for selective methanol-to-olefins. *Microporous Mesoporous Mater.* **2019**, *274*, 277–285. [CrossRef]
26. Dent, L.S.; Smith, J.V. Crystal Structure of Chabazite, a Molecular Sieve. *Nature* **1958**, *181*, 1794–1796. [CrossRef]
27. Nagy, J.B.; Gabelica, Z.; Debras, G.; Derouane, E.G.; Gilson, J.P.; Jacobs, P.A. ^{27}Al-n.m.r. characterization of natural and synthetic zeolites. *Zeolites* **1984**, *4*, 133–139. [CrossRef]
28. Akporiaye, D.E.; Dahl, I.M.; Mostad, H.B.; Wendelbo, R. Aluminum distribution in chabazite: An experimental and computational study. *J. Phys. Chem.* **1996**, *100*, 4148–4153. [CrossRef]
29. Mafra, L.; Vidal-Moya, J.A.; Blasco, T. Structural Characterization of Zeolites by Advanced Solid State NMR Spectroscopic Methods. In *Annual Reports on NMR Spectroscopy*; Academic Press Inc.: Cambridge, MA, USA, 2012; Volume 77, pp. 259–351. [CrossRef]
30. Yang, C.T.; Janda, A.; Bell, A.T.; Lin, L.C. Atomistic Investigations of the Effects of Si/Al Ratio and Al Distribution on the Adsorption Selectivity of n-Alkanes in Brønsted-Acid Zeolites. *J. Phys. Chem. C* **2018**, *122*, 9397–9410. [CrossRef]
31. Chen, K.; Gan, Z.; Horstmeier, S.; White, J.L. Distribution of Aluminum Species in Zeolite Catalysts: ^{27}Al NMR of Framework, Partially-Coordinated Framework, and Non-Framework Moieties. *J. Am. Chem. Soc.* **2021**, *143*, 6669–6680. [CrossRef] [PubMed]

32. Knott, B.C.; Nimlos, C.T.; Robichaud, D.J.; Nimlos, M.R.; Kim, S.; Gounder, R. Consideration of the Aluminum Distribution in Zeolites in Theoretical and Experimental Catalysis Research. *ACS Catal.* **2018**, *8*, 770–784. [CrossRef]
33. Weissenberger, T.; Machoke, A.G.; Bauer, J.; Dotzel, R.; Casci, J.L.; Hartmann, M.; Schwieger, W. Hierarchical ZSM-5 Catalysts: The Effect of Different Intracrystalline Pore Dimensions on Catalyst Deactivation Behaviour in the MTO Reaction. *ChemCatChem* **2020**, *12*, 2461–2468. [CrossRef]
34. Bates, S.A.; Delgass, W.N.; Ribeiro, F.H.; Miller, J.T.; Gounder, R. Methods for NH_3 titration of Brønsted acid sites in Cu-zeolites that catalyze the selective catalytic reduction of NOx with NH_3. *J. Catal.* **2014**, *312*, 26–36. [CrossRef]
35. Leistner, K.; Xie, K.; Kumar, A.; Kamasamudram, K.; Olsson, L. Ammonia Desorption Peaks Can Be Assigned to Different Copper Sites in Cu/SSZ-13. *Catal. Lett.* **2017**, *147*, 1882–1890. [CrossRef]
36. Fan, C.; Chen, Z.; Pang, L.; Ming, S.; Zhang, X.; Albert, K.B.; Liu, P.; Chen, H.; Li, T. The influence of Si/Al ratio on the catalytic property hydrothermal stability of Cu-SSZ-13 catalysts for NH_3-SCR. *Appl. Catal. A Gen.* **2018**, *550*, 256–265. [CrossRef]
37. Luo, J.; Gao, F.; Kamasamudram, K.; Currier, N.; Peden, C.H.F.; Yezerets, A. New insights into Cu/SSZ-13 SCR catalyst acidity. Part I: Nature of acidic sites probed by NH_3 titration. *J. Catal.* **2017**, *348*, 291–299. [CrossRef]
38. Gao, F.; Washton, N.M.; Wang, Y.; Kollár, M.; Szanyi, J.; Peden, C.H.F. Effects of Si/Al ratio on Cu/SSZ-13 NH_3-SCR catalysts: Implications for the active Cu species and the roles of Brønsted acidity. *J. Catal.* **2015**, *331*, 25–38. [CrossRef]
39. Chen, B.; Xu, R.; Zhang, R.; Liu, N. Economical way to synthesize SSZ-13 with abundant ion-exchanged Cu^+ for an extraordinary performance in selective catalytic reduction (SCR) of NOx by ammonia. *Environ. Sci. Technol.* **2014**, *48*, 13909–13916. [CrossRef] [PubMed]
40. Richter, M.; Fait, M.; Eckelt, R.; Schreier, E.; Schneider, M.; Pohl, M.-M.; Fricke, R. Oxidative gas phase carbonylation of methanol to dimethyl carbonate over chloride-free Cu-impregnated zeolite Y catalysts at elevated pressure. *Appl. Catal. B Environ.* **2007**, *73*, 269–281. [CrossRef]
41. Sultana, A.; Nanba, T.; Haneda, M.; Sasaki, M.; Hamada, H. Influence of co-cations on the formation of Cu^+ species in Cu/ZSM-5 and its effect on selective catalytic reduction of NOx with NH_3. *Appl. Catal. B Environ.* **2010**, *101*, 61–67. [CrossRef]
42. Cheng, J.; Han, S.; Ye, Q.; Cheng, S.; Kang, T.; Dai, H. Effects of hydrothermal aging at high and low temperatures on the selective catalytic reduction of NO_x with NH_3 over Cu/SAPO-34. *Res. Chem. Intermed.* **2019**, *45*, 2023–2044. [CrossRef]
43. Kwak, J.H.; Zhu, H.; Lee, J.H.; Peden, C.H.F.; Szanyi, J. Two different cationic positions in Cu-SSZ-13? *Chem. Commun.* **2012**, *48*, 4758–4760. [CrossRef]
44. Jangjou, Y.; Do, Q.; Gu, Y.; Lim, L.-G.; Sun, H.; Wang, D.; Kumar, A.; Li, J.; Grabow, L.C.; Epling, W.S. Nature of Cu Active Centers in Cu-SSZ-13 and Their Responses to SO_2 Exposure. *ACS Catal.* **2018**, *8*, 1325–1337. [CrossRef]
45. Corma, A.; Palomares, A.; Márquez, F. Determining the Nature of the Active Sites of Cu-Beta Zeolites for the Selective Catalytic Reduction (SCR) of $NO_x$by Using a Coupled Reaction-XAES/XPS Study. *J. Catal.* **1997**, *170*, 132–139. [CrossRef]
46. Ye, Q.; Wang, L.; Yang, R.T. Activity, propene poisoning resistance and hydrothermal stability of copper exchanged chabazite-like zeolite catalysts for SCR of NO with ammonia in comparison to Cu/ZSM-5. *Appl. Catal. A Gen.* **2012**, *427–428*, 24–34. [CrossRef]
47. Vovchok, D.; Tata, J.; Orozco, I.; Zhang, F.; Palomino, R.M.; Xu, W.; Harper, L.; Khatib, S.J.; Rodriguez, J.A.; Senanayake, S.D. Location and chemical speciation of Cu in ZSM-5 during the water-gas shift reaction. *Catal. Today* **2019**, *323*, 216–224. [CrossRef]
48. Shpiro, E.S.; Grünert, W.; Joyner, R.W.; Baeva, G.N. Nature, distribution and reactivity of copper species in over-exchanged Cu-ZSM-5 catalysts: An XPS/XAES study. *Catal. Lett.* **1994**, *24*, 159–169. [CrossRef]
49. Zhao, H.; Chen, X.; Bhat, A.; Li, Y.; Schwank, J.W. Applied Catalysis B: Environmental Insight into hydrothermal aging effect on deactivation of Pd/SSZ-13 as low-temperature NO adsorption catalyst: Effect of dealumination and Pd mobility. *Appl. Catal. B Environ.* **2021**, *286*, 119874. [CrossRef]
50. Usui, T.; Liu, Z.; Igarashi, H.; Sasaki, Y.; Shiramata, Y.; Yamada, H.; Ohara, K.; Kusamoto, T.; Wakihara, T. Identifying the Factors Governing the Early-Stage Degradation of Cu-Chabazite Zeolite for NH_3-SCR. *ACS Omega* **2019**, *4*, 3653–3659. [CrossRef]
51. Kim, Y.J.; Lee, J.K.; Min, K.M.; Hong, S.B.; Nam, I.S.; Cho, B.K. Hydrothermal stability of CuSSZ13 for reducing NOx by NH_3. *J. Catal.* **2014**, *311*, 447–457. [CrossRef]
52. De-La-Torre, U.; Pereda-Ayo, B.; Moliner, M.; González-Velasco, J.R.; Corma, A. Cu-zeolite catalysts for NOx removal by selective catalytic reduction with NH_3 and coupled to NO storage/reduction monolith in diesel engine exhaust aftertreatment systems. *Appl. Catal. B Environ.* **2016**, *187*, 419–427. [CrossRef]
53. Putluru, S.S.R.; Schill, L.; Jensen, A.D.; Fehrmann, R.S.N. Selective Catalytic Reduction of NOx with NH_3 on Cu-, Fe-, and Mn-Zeolites Prepared by Impregnation: Comparison of Activity and Hydrothermal Stability. *J. Chem.* **2018**, *2018*, 8614747. [CrossRef]
54. Palčić, A.; Bruzzese, P.C.; Pyra, K.; Bertmer, M.; Góra-Marek, K.; Poppitz, D.; Pöppl, A.; Gläser, R.; Jabłońska, M. Nanosized Cu-SSZ-13 and Its Application in NH_3-SCR. *Catalysts* **2020**, *10*, 506. [CrossRef]
55. Kim, D.H.; Kwon, D.W.; Hong, S.C. Structural characteristics of V-based catalyst with Sb on selective catalytic NOx reduction with NH_3. *Appl. Surf. Sci.* **2021**, *538*, 148088. [CrossRef]
56. Bartholomew, C.H. Mechanisms of catalyst deactivation. *Appl. Catal. A Gen.* **2001**, *212*, 17–60. [CrossRef]
57. Ma, J.; Si, Z.; Weng, D.; Wu, X.; Ma, Y. Potassium poisoning on Cu-SAPO-34 catalyst for selective catalytic reduction of NOx with ammonia. *Chem. Eng. J.* **2015**, *267*, 191–200. [CrossRef]

58. Cao, X.; Wan, B.; Liu, H.; Wu, L.; Yao, Y.; Gou, H. Potassium-activated anionic copper and covalent Cu–Cu bonding in compressed K–Cu compounds. *J. Chem. Phys.* **2021**, *154*, 134708. [CrossRef]
59. Xue, J.; Wang, X.; Qi, G.; Wang, J.; Shen, M.; Li, W. Characterization of copper species over Cu/SAPO-34 in selective catalytic reduction of NOx with ammonia: Relationships between active Cu sites and de-NOx performance at low temperature. *J. Catal.* **2013**, *297*, 56–64. [CrossRef]